Topside ionospheric irregularities as seen from multisatellite observations

Irina Zakharenkova, Elvira Astafyeva

RESEARCH ARTICLE

Key Points:
- Mapping of ionospheric irregularities from CHAMP onboard GPS measurements
- Most intense irregularities are detected at high and low latitudes
- High-latitude irregularities show asymmetry over northern and southern poles

Topside ionospheric irregularities as seen from multisatellite observations

Irina Zakharenkova[1] and Elvira Astafyeva[1]

[1]Institut de Physique du Globe de Paris, Paris Sorbonne Cite, Université Paris Diderot, Paris CEDEX, France

Abstract We use in situ data from CHAMP and DMSP satellites, along with data of GPS receiver onboard CHAMP satellite and ground-based GPS receivers to study the occurrence and global distribution of ionospheric irregularities during the main phase of the geomagnetic storm of 29–31 August 2004 (minimum *Dst* excursion of $-128\,nT$). Using the CHAMP GPS measurements, we created maps of GPS phase fluctuation activity and found two specific zones of the most intense irregularities: (1) the region of the auroral oval at high latitudes of both hemispheres and (2) the low latitudes/equatorial region between Africa and South America. At high latitudes, the topside ionospheric irregularities appeared to be more intensive in the southern hemisphere, which is, most likely, due to seasonal variations in the interhemispheric field-aligned currents system. An analysis of multi-instrumental observations reveals reinforcement of the equatorial ionization anomaly after sunset in Atlantic sector on 30 August and formation of the significant plasma depletions and irregularities over a large longitudinal range. Equatorial irregularities were also found in the morning sector at the recovery phase of the storm. In addition to low Earth orbit (LEO) GPS measurements, we analyze the LEO in situ measurements, and we show that these two techniques cannot be interchangeable in all cases because of the altitudinal extent of plasma irregularities. Overall, we demonstrate that the LEO GPS technique can serve a useful tool for detection of the topside ionospheric irregularities during space weather events and may essentially contribute to other methods based on various instruments.

1. Introduction

Extensive experimental research of the ionospheric irregularities occurrence, as well as theoretical studies on the plasma instability processes, has been reported in the scientific literature [e.g., *Dyson and Benson*, 1978; *Fejer and Kelley*, 1980; *Keskinen and Ossakow*, 1983; *Kersley et al.*, 1995; *Jakowski et al.*, 2012; *Hysell et al.*, 2013]. Ionospheric irregularities generated mainly at the bottomside ionosphere can develop in time and space; as a result, the ionospheric irregularity region vertically extends to high altitudes, at least 2000–3000 km [e.g., *Phelps and Sagalyn*, 1976; *Su et al.*, 2006]. As it was stated by *Woodman* [1993], the topside irregularities are always originated in the linearly unstable bottomside ionosphere. In particular, the cause of the equatorial spread *F* event, or so called after *Kelley et al.* [2011] convective ionospheric storm, is related to density irregularity structures resulted from a multistep nonlinear plasma process initiated from the large-scale gravitational Rayleigh-Taylor (R-T) instability at the bottomside ionosphere [e.g., *Keskinen et al.*, 1980; *Ossakow*, 1981; *Kuo et al.*, 1998]; however, it does not require that the bottomside R-T instability to be the ultimate source for all or any kind of the topside irregularities [*Fejer and Kelley*, 1980]. Next region with the most intense ionospheric irregularities is the high-latitude ionosphere, a highly structured medium containing irregularities that are mostly caused by plasma processes associated with auroral activities, attributed to energetic particle precipitation, and dynamical processes including high-speed plasma convection [e.g., *Fejer and Kelley*, 1980; *Keskinen and Ossakow*, 1983].

While the ionospheric irregularities of the bottomside ionosphere and *F* region in the equatorial and auroral regions have been extensively studied with the wide range of ground-based measuring facilities such as ionosondes, incoherent scatter radars, VHF/HF coherent backscatter radars, all-sky cameras, and GPS stations [e.g., *Rodger and Jarvis*, 2000], investigations of the topside ionospheric irregularities are mostly limited by ground-based radars and in situ observations using probes carried by low Earth orbit (LEO) satellites. As known, each instrument has its own limitations. There are only few incoherent scatter radars in the world, and generally, due to expensive costs, their measuring campaigns are limited in time (several days per month). Satellite measurements can provide in situ plasma density probe but at the specific altitude range depending on the satellite orbit, e.g., CHAMP at ~400 km, ROCSAT-1 at ~600 km, DMSP at ~850 km, and C/NOFS at

~400 × 850 km due to the elliptical orbit. The undoubted advantage of LEO satellites with a polar orbit is the principal possibility to get continuous data over all latitudes, as well as over regions with total lack of ground-based measuring facilities like oceans and deserts. Therefore, these satellites give us information on the plasma density at a specific point of orbit track, but what happens at the same time above this orbit? Can irregularities, detected with the in situ measurements, dissipate simultaneously or still persist at the topside ionosphere? There is still an extremely low probability to observe two LEO satellites flying one above the other at the same sector and time. The chance to look upward together with the in situ measurements can be realized only with another instrument of a satellite payload, for example, zenith GPS antenna. The majority of the modern LEO satellites is equipped with the dual-frequency GPS receivers, and zenith-looking antenna can be used not only for the precise orbit determination (POD) but can also provide valuable information on the ionization state of the topside ionosphere and plasmasphere above the satellite orbit [e.g., *Heise et al.*, 2002]. Here we present the first results provided by LEO GPS technique on detection of the ionospheric irregularities above the CHAMP orbit and compare them with simultaneous in situ measurements of the electron density by the Langmuir probe onboard CHAMP.

The main purpose of this paper is to investigate the occurrence of the ionospheric irregularities on a global scale during the geomagnetic storm on 29–31 August 2004 using multi-instrumental observations. The morphology and the occurrence location of the plasma density irregularities are examined by using the in situ measurements of CHAMP and DMSP satellites, as well as observations from ground-based GPS receivers. The second purpose of this research is to demonstrate that GPS phase fluctuation measurements from the GPS receiver onboard LEO satellites can be an effective tool for monitoring the occurrence of the topside ionospheric irregularities and may essentially contribute to the multi-instrumental analysis of the ground-based and in situ data. This work presents the global picture of the ionospheric irregularities detection using GPS phase fluctuation measurements, namely, ROT as time rate of change of the GPS differential carrier phase, but, to our knowledge, for the first time attention will be directed to ROT observations from GPS receiver onboard LEO satellite. We discuss first results that provide this technique to detect the electron density irregularities at the topside ionosphere above the CHAMP orbit from GPS signal measurements under geomagnetically quiet and disturbed conditions.

2. The Study Period, 29–31 August 2004

Geomagnetic storm, occurred on 29–31 August 2004, was rather moderate one in comparison with other severe geomagnetic events during the years 2003 and 2004; however, it can be considered as an intensive storm according to the maximum *Dst* index variations below −100 nT [*Gonzalez et al.*, 1994]. An interplanetary shock was observed at ~09:00 UT on 29 August by the Advanced Composition Explorer, which gives the time of sudden storm commencement (SSC) of 10:04 UT on the Earth (vertical dashed line in Figure 1). With the shock arrival, an abrupt increase of the solar wind speed was observed, along with sudden changes in solar wind ram pressure and proton density (Figure 1). The interplanetary magnetic field (IMF) B_Z component showed a smooth rotation, indicating a magnetic cloud [*Echer et al.*, 2008, Figure 1]. The geomagnetic storm had a long and monotonic development before the peak of *SYM-H*, which occurred at 22:00 UT on 30 August (minimum *SYM-H* excursion of −128 nT). The auroral electrojet (indicated by *AE* index) showed a small short-term increase ~4 h after the shock arrival on 29 August. However, much more prominent enhancement in the *AE* activity was observed from ~05 UT to 23 UT on 30 August, when the IMF B_Z turned southward and remained that for many hours. Consequently, the substorm activity remained highly enhanced (with *AE* up to 1000–1200 nT) from 09 to 23 UT on 30 August and further continued during many hours on 31 August (Figure 1). The recovery phase lasted almost 5 days.

3. Data Set

Multi-instrumental data set was used in this research. Most important results come from CHAMP measurements. The in situ electron density at ~400 km height was obtained from CHAMP planar Langmuir probe (PLP) measurements [*Reigber et al.*, 2002]. The data of the POD antenna of the onboard GPS receiver were used to determine the total electron content (TEC) between CHAMP and GPS satellites, viz., topside
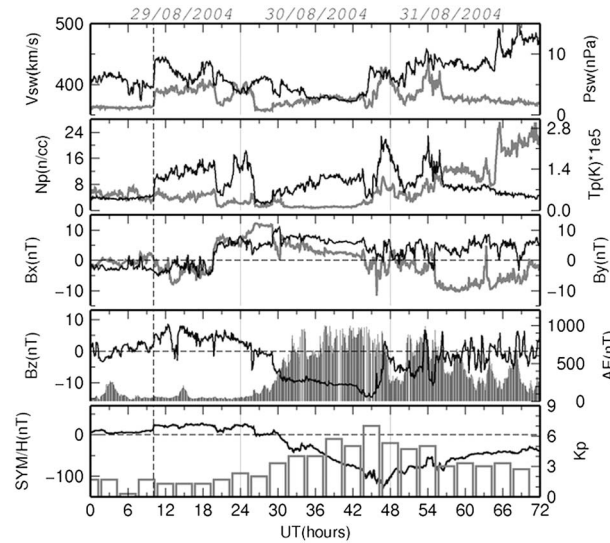
Figure 1. Variations of interplanetary and geomagnetic parameters during 29–31 August 2004 geomagnetic storm (from OMNIWeb Plus services, http://omniweb.gsfc.nasa.gov/). The vertical dashed line shows the SSC time (10:04 UT); the vertical gray lines separate 3 days under consideration. (top to bottom) Solar wind speed (V_{sw}, black curve) and solar wind ram pressure (P_{sw}, gray curve), proton density (N_p, black) and proton temperature (T_p, gray), B_X (black) and B_Y (gray) components of the interplanetary magnetic field, IMF B_Z component (black) in GSM coordinates and geomagnetic auroral electrojet index (AE, gray bars), and index of geomagnetic activity SYM-H (black curve) and planetary index Kp (gray bars). All parameters are 5 min averaged (except for 3 h index Kp).

ionosphere/plasmasphere electron content in the altitudinal range of 400–20,200 km. The ion concentration Ni at ~840 km height was obtained from the in situ plasma measurements by DMSP F15 satellite (DMSP F15 platform document, 2008, http://nsidc.org/data/docs/daac/f15_platform.gd.html). GPS TEC from ground-based stations was obtained using International Global Navigation Satellite Systems (GNSS) Service (IGS) network.

4. GPS Data Analysis

Ionospheric irregularities can be characterized by measuring their impact on the amplitude and phase of the received GPS signal. In order to estimate slant TEC from the frequency-differenced GPS phase delay, the well-known algorithms were used from *Blewitt* [1990] and *Hofmann-Wellenhof* [2001]. During phase TEC processing, detection and correction of cycle slips, loss of lock, and multipath were done.

Pi et al. [1997] proposed to use the time derivative of TEC (ROT, rate of TEC change) as a measure of phase fluctuation activity and the rate of TEC index (ROTI) as a GPS-based index that characterizes the severity of the GPS phase fluctuations and detects the presence of ionospheric irregularities, as well as measures the irregular structures of TEC spatial gradient. ROT is calculated using the algorithm (equation (1)):

$$ROT = \frac{TEC_k^i - TEC_{k-1}^i}{(t_k - t_{k-1})} \tag{1}$$

where *i* is a visible satellite and *k* is the time of epoch. The CHAMP receiver-independent exchange (RINEX) files raw data that are sampled at 10 s. ROT is calculated in units of total electron content unit (TECU)/min, where 1 TECU = 10^{16} el/m², for each visible GPS satellite at CHAMP position. The ROT values are then calculated and detrended for all individual satellite tracks for elevation angles over 50°. Based on the retrieved values of ROT, the ROTI values are calculated over 1 min period with running window (equation (2)):

$$ROTI = \sqrt{\langle ROT^2 \rangle - \langle ROT \rangle^2} \tag{2}$$

Here we used a thin-layer model based on the assumption that all electrons are concentrated in an infinitely thin spherical shell at 450 km of height; the locations of the phase fluctuations are related to the locations of the ionosphere piercing points. Along the satellite pass, we use a grid of 1°×5° resolution in latitude and longitude correspondingly. The value in every cell is calculated by averaging all ROTI values in the cell area.

It should be noted that the ROT/ROTI technique by the ground-based GPS observations is widely used to track signatures of the ionospheric irregularities and their influence on the performance of navigation systems [e.g *Pi et al.*, 1997; *Aarons and Lin*, 1999; *Nishioka et al.*, 2008; *Maruyama et al.*, 2013; *Cherniak et al.*, 2014; *Astafyeva et al.*, 2014]. Results of the ROTI technique applied to LEO GPS observations were not yet reported.

In contrast to the ROTI technique from LEO GPS measurements, the topside vertical TEC above LEO orbit is often used to study the topside ionospheric density; in particular, due to low CHAMP orbit, the observations of CHAMP POD vertical total electron content (VTEC) is of high importance [e.g., *Heise et al.*, 2002; *Mannucci et al.*, 2005; *Yizengaw et al.*, 2006; *Astafyeva*, 2009a, 2009b]. To estimate vertical TEC from CHAMP GPS measurements,

first,we calculate the slant TEC obtained from pseudorange measurements; then to obtain the absolute slant TEC, we use a phase-leveling code algorithm described in *Ma and Maruyama* [2003]. The retrieved slant TEC should be calibrated from instrumental biases. Differential code biases (DCB) for GPS satellites are used from the final IGS global ionosphere map product. To estimate the unknown DCB for CHAMP receiver, we apply algorithm generally used in University Corporation for Atmospheric Research Constellation Observing System for Meteorology, Ionosphere, and Climate (COSMIC) Data Analysis and Archive Center (UCAR CDAAC) for LEO GPS data processing [*Yue et al.*, 2011]. Slant TEC values were scaled to estimate vertical POD TEC using a geometric factor derived by assuming the plasma occupies a spherical thin shell at the altitude of 450 km. The elevation angle cutoff was selected as 50°. In the case when several GPS satellites were above the cutoff angle, the values of vertical TEC were averaged to obtain a single POD VTEC value for each epoch.

5. Results

5.1. Overall View on the Ionospheric Irregularities at the Topside Ionosphere From CHAMP GPS Data

We examine spatial-temporal variation of the ionospheric irregularities observed in GPS phase fluctuations by using CHAMP GPS measurements. To the best of our knowledge, attention has never been paid on ROT/ROTI observations from GPS receiver onboard LEO satellite. Figure 2 presents the global maps of the ROTI variability along CHAMP passes during 30–31 August 2004 and average ROTI maps for (left) the evening postsunset and (right) morning sectors. All passes are shown in chronological order from right to left. Approximate time of the geographic equator crossing time in universal time (UT) is indicated at the top part of each graph; the equator crossing time in local time (LT) was about 21:00 LT for the evening sector and 09:00 LT for the morning sector. Maps are presented in geographic coordinates. The data gaps are due to either missing of GPS observations in RINEX file or no GPS satellites being above 50° elevation angle.

As a reference source for the quiet time, Figures 2a and 2d present the average maps calculated from CHAMP ROTI observations from the set of 14 quiet days in August 2004 before the considered event. The average ROTI map is constructed with grid sectors of 5°×10° resolution in latitude and longitude correspondingly; the value in every cell is calculated by averaging all ROTI values covered by this cell area. Average ROTI map for the morning sector (Figure 2d) illustrates a very low intensity of fluctuation activity with higher values observed at high latitudes, whereas for the evening sector (Figure 2a), one can observe more intense level of fluctuation activity with increased ROTI values at high and equatorial latitudes.

Next graphs (Figures 2b, 2c, 2e, and 2f) illustrate the maps with separate CHAMP ROTI passes during 30–31 August 2004. We observe a significant increase of the fluctuation activity level during the prolonged main phase of the storm, practically on the whole day of 30 August. As the CHAMP altitude was ~400 km, the detected GPS phase fluctuations were related to plasma irregularities at the topside ionosphere. The occurrence of the most intense ionospheric irregularities can be seen as regions with the very high ROTI (equal to 5 and higher) values. We can clearly observe two specific zones of the most intense irregularities —first is the region of the auroral oval at high latitudes of both hemispheres and the second one is the low latitudes/equatorial region between Africa and South America. Comparison between the observed irregularities and the reference quiet time maps reveals considerably higher level of the intensity as well as the expansion of the areas affected by the irregularities occurrence. In the next sections, we demonstrate the reliability of the ROTI-detected ionospheric irregularities by comparison with independent instrument measurements.

5.2. Ionospheric Irregularities at High Latitudes

As mentioned above, Figure 2 demonstrates much higher intensity of ROTI-detected ionospheric irregularities in the southern auroral and subauroral zones; the intensity increased for those CHAMP passes that were located closer to the southern magnetic pole.

Figures 3 and 4 illustrate the comparison of in situ measurements for CHAMP electron density Ne at altitude ~400 km and DMSP ion density Ni at altitude ~840 km for northern and southern hemispheres, respectively, for the disturbed day of 30 August 2004. We selected CHAMP and DMSP passes that were closest to one another in space and time, i.e., with minimal angle between the orbit planes. However, some temporal shift between CHAMP and DMSP passes should be taken into account. CHAMP data are indicated on the graphs by red color, and DMSP data are indicated by blue color. Each graph contains polar view with projection of
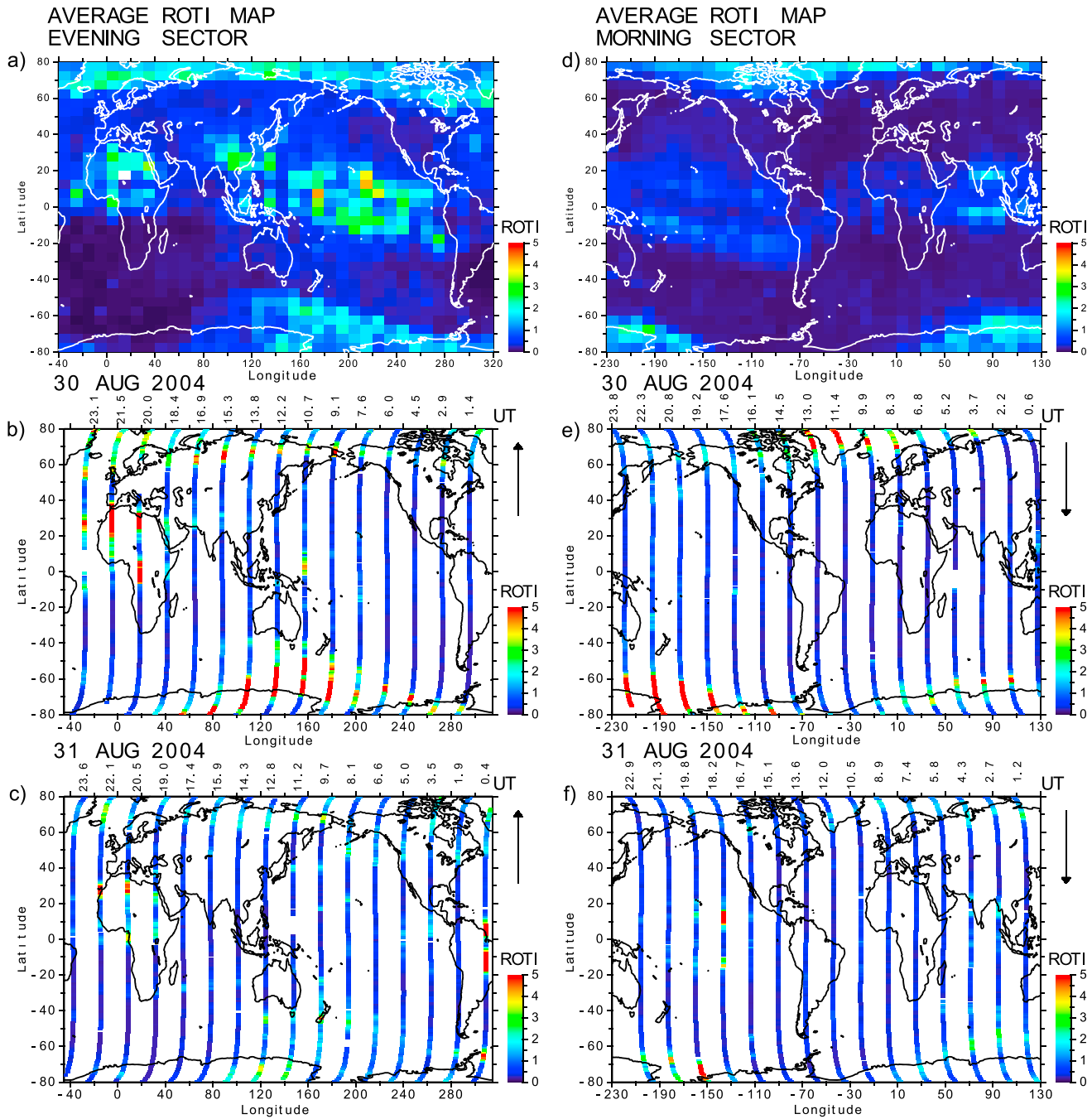
Figure 2. Global maps of CHAMP ROTI observations. Global maps of the ROTI variability along CHAMP passes on 30–31 August 2004 for (a–c) evening and (d–f) morning (right panel) sectors. (a and d) Average ROTI maps for quiet time period. All passes are shown in chronological order from right to left. Approximate time of equator crossing time in UT is indicated at the top part of each graph; the equator crossing time in LT was about 21 LT for evening sector and 09 LT for morning sector. The maps are presented in geographic coordinates.

satellite pass in geographical coordinates and variability of plasma density along this pass, marked by a corresponding color. Information about corresponding UT, LT, and geographic and magnetic coordinates are noted at the top (for CHAMP) and bottom (for DMSP) axes. Minutes are indicated in decimal format.

We can note that despite the fact that these in situ observations are separated by ~450 km in altitude and densities of the ionospheric plasma at these altitudes are quiet different, the variations of Ne and Ni are rather comparable and similar in absolute values of deviations.
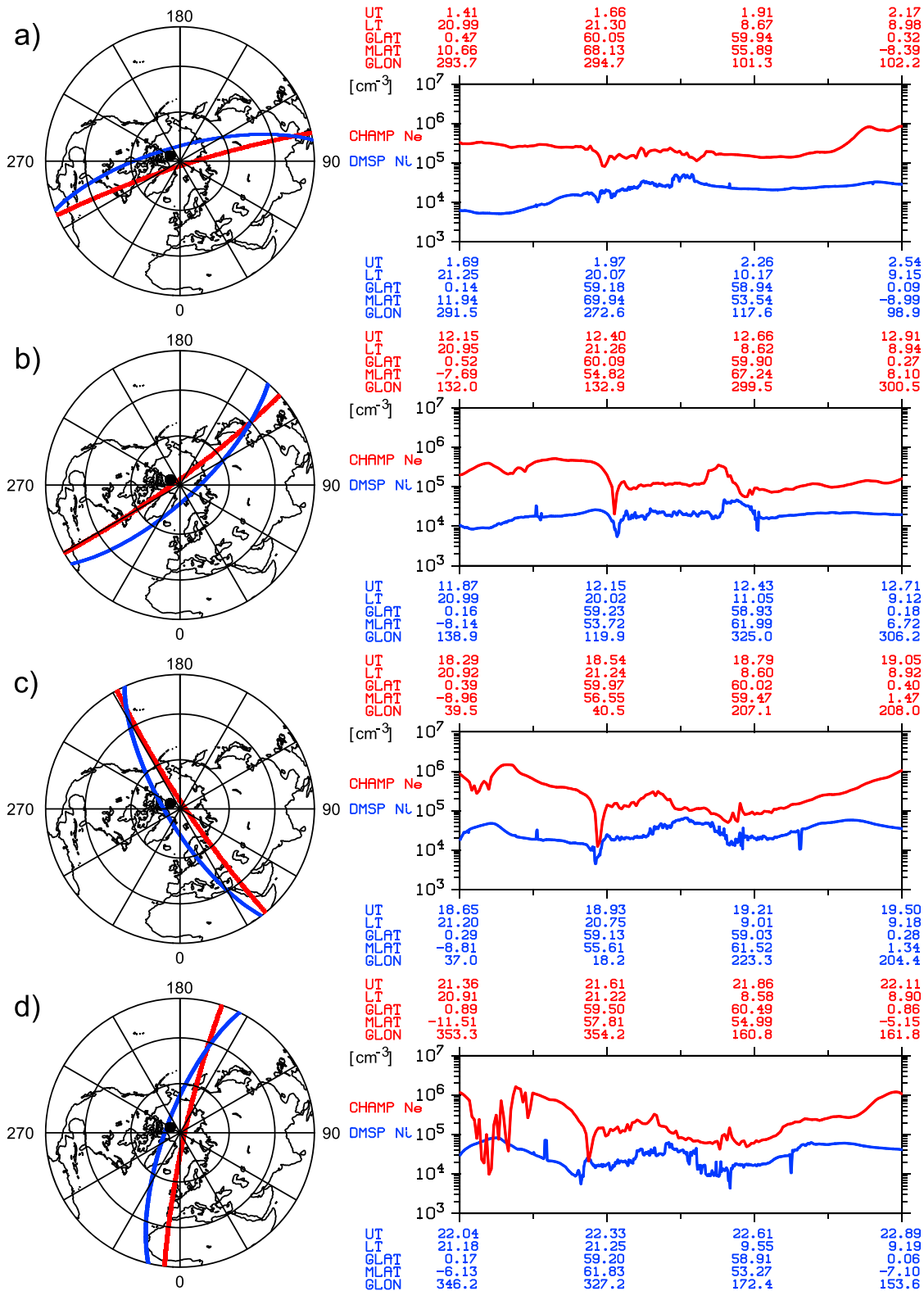
Figure 3. Comparison of in situ measurements for CHAMP Ne at altitude ~400 km and DMSP Ni at altitude ~840 km for northern hemisphere for the disturbed day of 30 August 2004. CHAMP data are indicated on the graphs by red color, and DMSP data are indicated by blue color. Each graph contains polar view with projection of satellite pass in geographical coordinates and variability of plasma density along this pass, marked by corresponding color. Information about corresponding UT, LT, and geographic and magnetic coordinates are noted at the top (for CHAMP) and bottom (for DMSP) axes. Minutes are indicated in decimal format. The black dot indicates the position of magnetic pole.
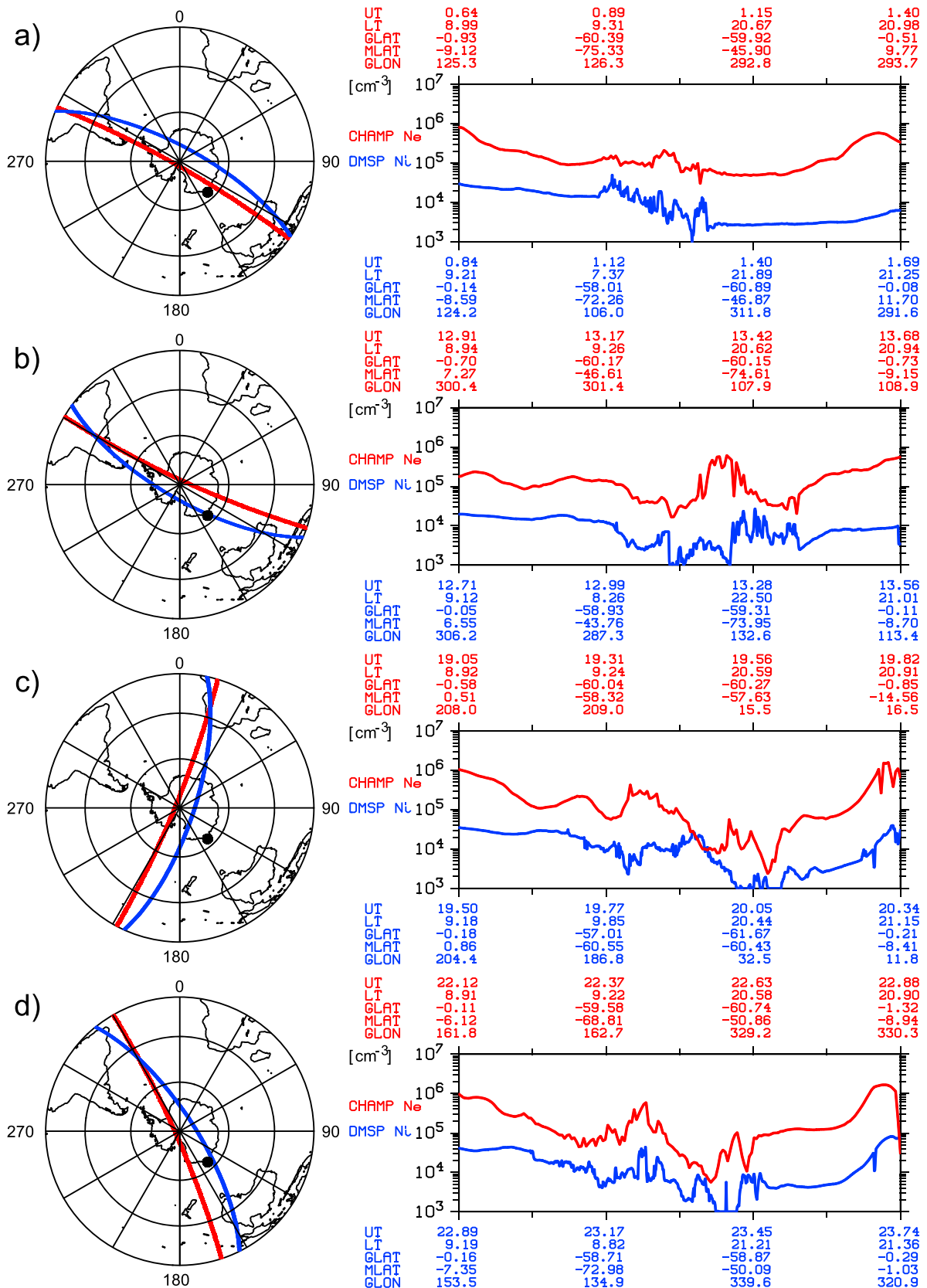
Figure 4. Same as Figure 3 but for southern hemisphere.

In fact, we observe clear asymmetry between the northern and southern hemispheres; i.e., variations of plasma density were considerably more intensive over the southern pole. When the IMF B_Z was southward, weak or no significant plasma density variations were detected in the northern polar cap, while in the southern polar cap, rapid variations of plasma density persisted for many hours. The general pattern of this variability was rather similar in both altitudinal regions.

The prominent peculiarity, observed at the topside plasma density over the northern hemisphere, is the precise deepening of the midlatitude ionospheric trough in the evening sector. As known, one of the most significant changes in the trough during storm periods is the equatorward movement of the trough location. Figure 3a indicates the presence of the trough in both plasma density measurements at about 68° magnetic latitude (MLAT). With the intensification of geomagnetic activity, the trough was observed at 54°–56° MLAT for the evening postsunset conditions (Figures 3b–3d). We can suggest that CHAMP ROTI-detected ionospheric irregularities observed in the northern hemisphere are related mainly with the rapid gradients of the ionospheric plasma density at the edges of the midlatitude ionospheric trough. The sharp density change at the trough's poleward edge is explained by the plasma density enhancement on the auroral oval induced by the energetic particle precipitation and transport of the dayside plasma, whereas the equatorward edge of the ionospheric trough is a region where the plasma can be unstable due to the temperature-gradient instability [*Rodger et al.*, 1992].

It is interesting to note that Figure 3d demonstrates also the occurrence of strong plasma density depletions at equatorial latitudes after 21:30 UT at the altitude of 400 km; however, these depletions did not reach the DMSP altitude of 840 km. Peculiarities of the ionospheric irregularities occurrence in low-latitude region will be discussed in the next section.

In the southern hemisphere, more complicated situation is found (Figures 4a–4d). We observe much higher in amplitude and more dynamic variations of both Ne and Ni, as compared to those over the northern polar region. The zone of the strong plasma density variation enlarged equatorward with the increase of the geomagnetic storm intensity. Large-scale ionospheric fluctuations in the form of increased/decreased values of plasma density were observed with CHAMP and DMSP in situ measurements. At both altitudes, the strength of the fluctuations reached amplitude up to a factor of 10.

Figure 5 represents the reference for comparison of the CHAMP and DMSP in situ observations for disturbed and quiet time conditions. We analyzed in details the cases for both hemispheres corresponded to Figure 3d and Figure 4d. Figures 5a–5c and Figures 5d–5f show the comparison for the northern and southern hemispheres, respectively. Figures 5b and 5e present the CHAMP Ne and Figures 5c and 5f the DMSP Ni. The black lines at these graphs show the values of quiet day (28 August 2004) and corresponded to the satellite traces marked by the asterisks at Figures 5a and 5d. Comparison for CHAMP Ne data over the northern hemisphere (Figure 5b) reveals rather smooth background state of the electron density at the high latitudes with the increase of fluctuation activity during the disturbance time; besides, we can observe the deepening and equatorward displacement of the main ionospheric trough at the local evening sector. There is the Ne increase at low latitude and midlatitude in evening sector observed in the data of CHAMP that is also seen in the DMSP Ni data (Figure 5c). However, the CHAMP Ne observations show the strong depletions in the equatorial region. An analysis of the DMSP data (Figures 5c and 5f) also demonstrates the increase of the plasma density up to an order of magnitude in equatorial and low-latitude region in the local evening sector. It is clearly seen that during quiet period, the ionospheric irregularities were registered in DMSP data close to the cusp of the southern pole. During the disturbed day, the most pronounce plasma density changes were observed within a wider region of latitudes of −70° MLAT that can be explained by particle precipitations and related processes.

5.3. Ionospheric Irregularities at Low Latitudes

The second zone of the ionospheric irregularities occurrence detected from CHAMP ROTI data (Figure 2) is the low latitudes/equatorial region between Africa and South America. These irregularities can be associated with the increase of the equatorial plasma density instabilities in the evening postsunset sector during the main phase of the geomagnetic storm.

In order to analyze the response of the equatorial ionosphere to the geomagnetic disturbance, we compare several CHAMP passes for the evening sector during the storm day of 30 August with a quiet day of 28 August.
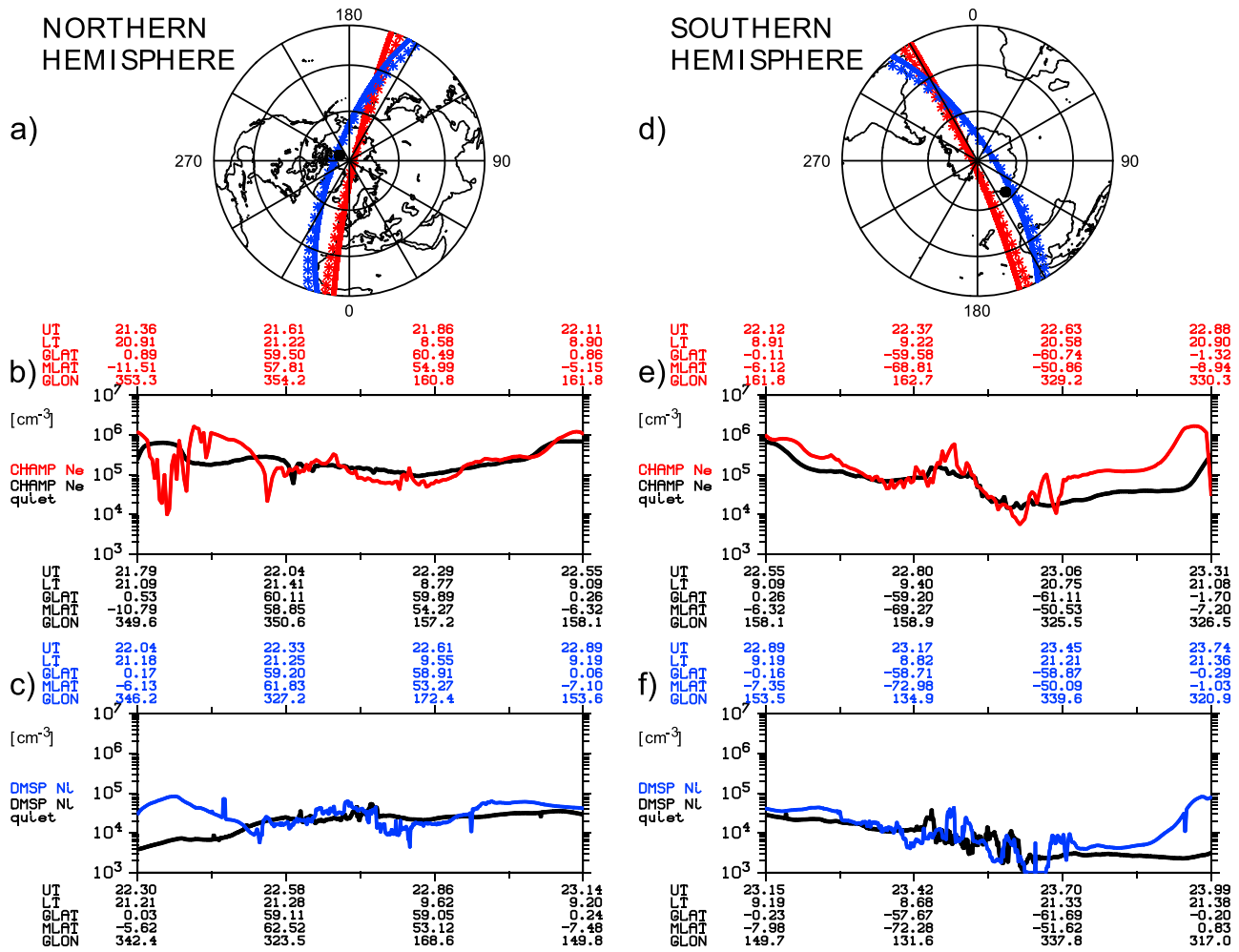
Figure 5. Reference comparison of CHAMP and DMSP in situ measurements for disturbed and quiet conditions (cases from Figures 3d and Figures 4d).

Figure 6 (top) shows the projection of these passes in geographical coordinates. Also on this map, we plot the position of several selected GPS ground-based receivers (black rhombuses). The graphs at Figure 6 (bottom) demonstrate the comparison of CHAMP measurements at these selected passes for quiet time (black line) versus disturbed time (red line). Figures 6 (left column) presents the in situ electron density Ne (altitude ~400 km); Figure 6 (right column) presents the CHAMP-derived POD VTEC (altitude range of 400–20,200 km). The most pronounced effects were observed for passes in Figures 6b–6f of each column, i.e., from ~18 UT to 24 UT. The in situ Ne measurements have clearly revealed the intensification of the equatorial ionization anomaly (EIA) in the evening postsunset sector, that is quite different from the quiet time plasma behavior (black lines) when the maximum Ne was observed near the magnetic equator. The increase of the Ne in the reintensified crests of EIA was of factor of 5–30 and was accompanied by the presence of the abrupt and deep plasma density depletions. We can note that POD VTEC, related to the topside electron content, demonstrates very similar behavior with the in situ Ne at the altitude of 400 km. One can observe the reintensification of the EIA for CHAMP traces in Figures 6b–6f of each column. It indicates the considerable increase of the topside electron density up to the factor of 5 at the northern crest of the EIA in comparison with normal distribution. The effect of the EIA reinforcement after sunset was observed within the limited zone between 60°W and 30°E.

Additionally, we analyze the ROT variability for several ground-based GPS receivers. We select two meridional chains of IGS stations in Africa and South America; positions of the stations are shown in Figure 6. Figure 7 shows the detrended ROT values for all GPS satellite passes over the stations during the period of 29–31 August 2004. The increase of the phase fluctuation activity was observed from 20–21 UT of 30 August to 04 UT
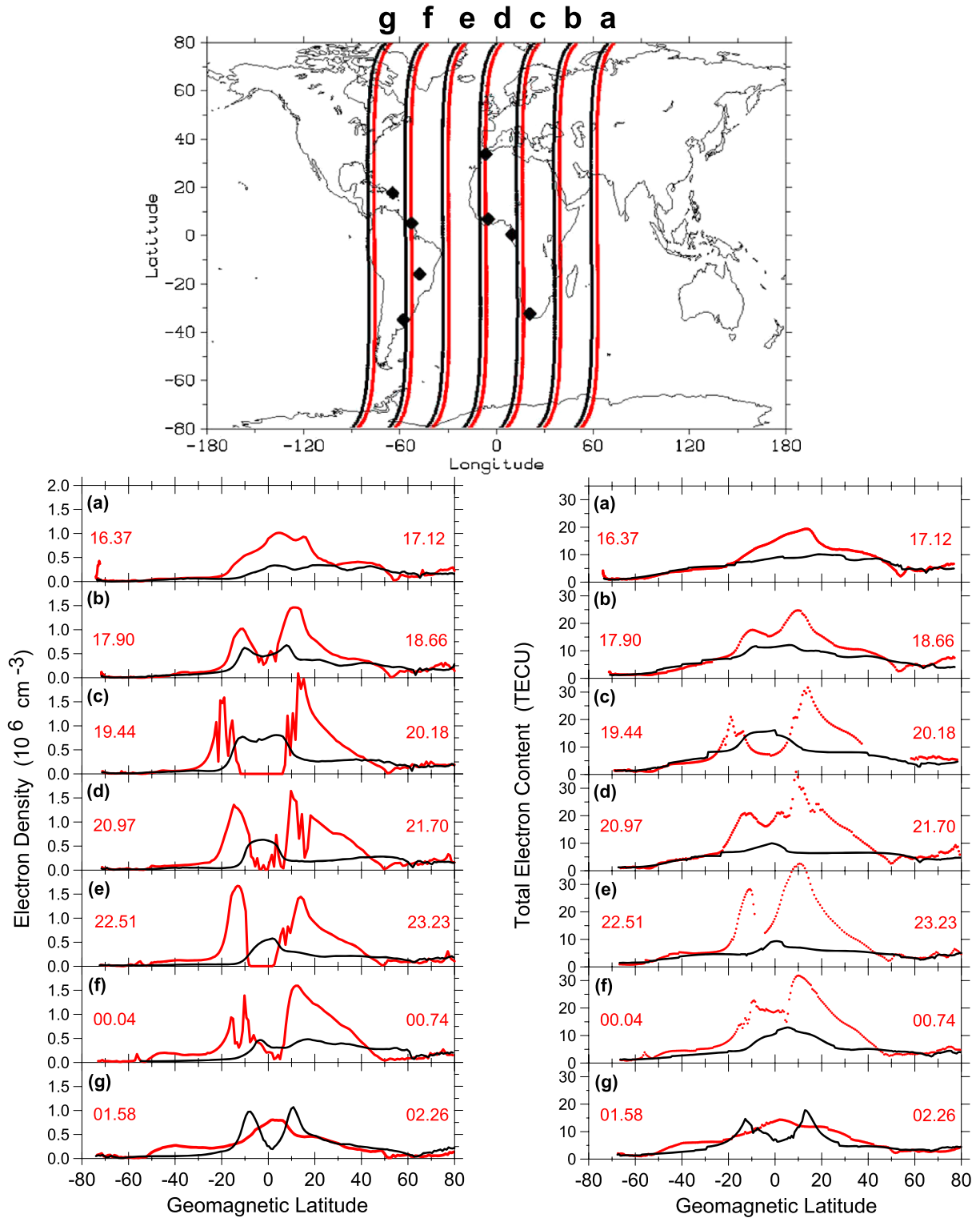
Figure 6. (top) Projection of selected CHAMP passes in geographical coordinates and the position of several GPS ground-based receivers, marked by black rhombuses. Comparison of CHAMP measurements along these selected passes for quiet time (black line) versus disturbed time (red line). (left column) The in situ electron density Ne (altitude ~400 km). (right column) CHAMP-derived POD VTEC (altitude range of 400–20,200 km).
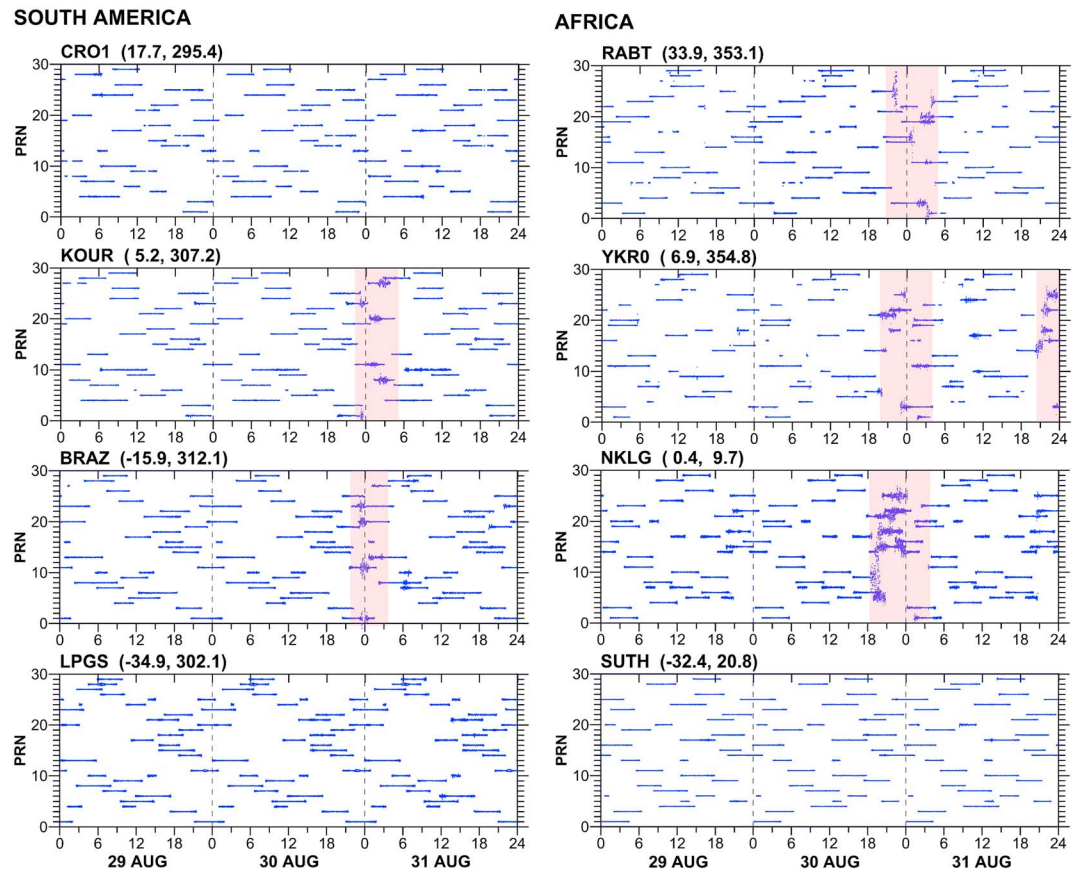
Figure 7. ROT variability during the period of 29–31 August 2004 for several ground-based GPS receivers in Africa and South America; positions of the stations are shown at Figure 6 (top).

of 31 August. This effect was limited in space and time and was not registered for all GPS stations. Moreover, for all these equatorial stations, we do not observe other GPS phase fluctuations during this geomagnetic storm, so that GPS phase fluctuations from the ground-based GPS stations confirm the presence of the ionospheric irregularities at low latitudes of the Atlantic sector as it was registered previously by the CHAMP ROTI data.

An analysis of multi-instrumental observations reveals significant reinforcement of the EIA after sunset in the Atlantic sector on 30 August. This effect was seen along CHAMP passes between 18 UT in both in situ electron density at 400 km and the topside total electron content observations. In situ data clearly indicate the presence of the deep plasma density depletions in the EIA region; at the same time, observations from the ground-based GPS receivers demonstrate local increase of phase fluctuations activity, related with the presence of ionospheric irregularities at the postsunset time.

Furthermore, we found that CHAMP ROTI technique registered also the occurrence of the increased ionospheric irregularities over equatorial latitudes of two CHAMP passes in the morning sector on 31 August 2004 (Figure 2f). In fact, the equatorial irregularities in the morning local time are not registered frequently. We compare results derived by CHAMP ROTI observations with CHAMP Ne density at the orbit altitude. Figure 8 (left) shows the sector with the CHAMP ROTI results, whereas Figure 8 (right) presents the in situ electron density along the corresponding CHAMP passes (red lines) but in comparison with quiet day of 28 August (black lines). An examination of CHAMP Ne data reveals the presence of the strong plasma density gradients over the equatorial regions of passes in Figures 8b and 8c (right). The geographical position of these gradients is practically identical to ones registered by CHAMP ROTI at Figure 8 (left). Also, there are geographical coincidence of the irregularities observed along passes in Figures 8c and 8d (left) at the high latitudes of the southern hemisphere.
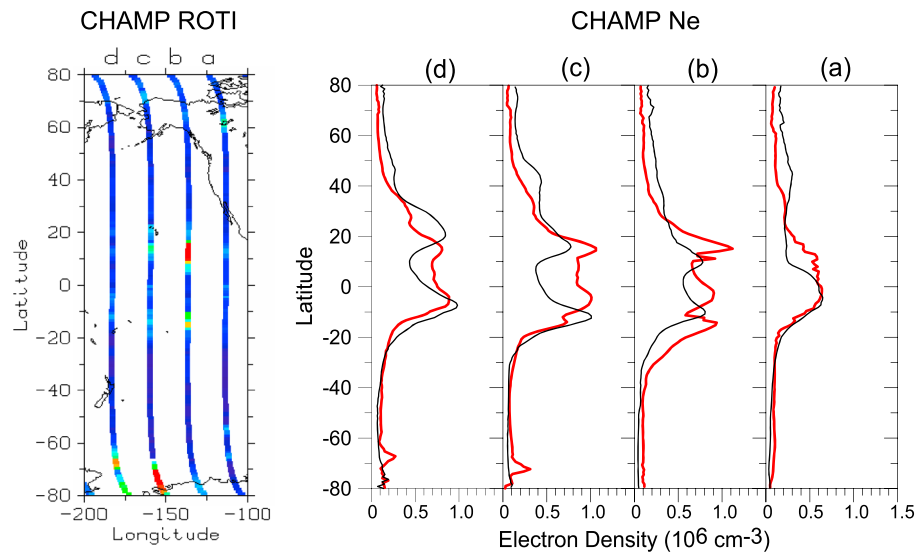
Figure 8. CHAMP ROTI and CHAMP Ne observations of the equatorial irregularities at the same orbit passes in the morning sector.

6. Discussion

6.1. Ionospheric Irregularities at High Latitudes

An analysis of CHAMP ROTI, CHAMP Ne, and DMSP Ni observations reveals clear asymmetry between the northern and southern hemispheres—variations of the high-latitude plasma density were more intensive over the southern pole. The observed asymmetry of the intensity of the plasma density fluctuations at high-latitude ionosphere cannot be fully explained by only one mechanism and is related to the complex of the plasma and dynamic processes that occurred in polar ionosphere during the main phase of geomagnetic disturbance. One of the possible explanations can be related to the magnetosphere asymmetry that leads to the displacement of conjugate areas in polar regions for summer and winter hemispheres [*Akasofu*, 1968]. As a result, particle precipitation can reach lower latitudes in southern hemisphere (local winter) than in northern hemisphere (local summer). *Liou et al.* [2001] reported that nightside (~19:00–03:00 magnetic local time) auroral power is suppressed in local summer and the average energy of precipitating electrons is higher in winter than in summer for the entire auroral oval.

It is known that the extended period of the southward IMF during the magnetic cloud passage can produce dynamic and intense polar precipitation. The increase in the magnetic storm intensity is accompanied by intensification of particle precipitation on the nightside and their drift around the Earth to the dawnside. *Yagodkina et al.* [2012] investigated global pattern of the auroral precipitation and dynamics of the precipitation boundaries during different intensity magnetic storms driven by magnetic clouds on the base of DMSP data and modeling simulations. They found a significant displacement to lower latitudes of both the diffuse auroral zone and the auroral oval precipitation region in the morning and evening sectors during the main phase of the storms. *Newell et al.* [1998] explained such asymmetry (the dawn-dusk widening of the precipitation zones) by changes in the configuration of the geomagnetic tail under storm conditions. In turn, particle precipitation is expected to play an important role in structuring the high-latitude *F* region of the ionosphere.

Lazutin et al. [2011] reported that ~1 month before the storm onset on 29 August 2004, the Earth's radiation belts were filled with enhanced flux of energetic particles, which were trapped and accelerated during the magnetic storms of 23–27 July 2004. *Lazutin et al.* [2011] showed that proton precipitation on 30 August caused a substantial depletion of the proton belt, predominantly near the loss cone. Proton precipitation lasted from 05 to 22 UT, i.e., from the beginning of the enhanced auroral activity and until the end of the storm's main phase. Large drop in the intensity of electrons with energy 3 MeV and higher was observed at *L* shell = 3.5; maximum amplitude of electron losses was of factor of 20. Consequently, we can expect significant intensification of particle precipitation and subsequent formation of large-scale plasma density enhancements in the high-latitude ionosphere.

Another source to drive various plasma instabilities in the high-latitude F region of the ionosphere is the magnetic field-aligned current (FAC) system [*Keskinen and Ossakow*, 1983]. *Lyatskaya et al*. [2008] found that substorm activity in summer correlates much better with geomagnetic activity not in the nearby polar cap but in the opposite polar cap. This effect can be caused by the interhemispheric FACs flowing from the summer high-latitude ionosphere and closing through the ionosphere on the opposite auroral zone. This leads to the decrease of the total FACs and their contribution to magnetic disturbances in the summer hemisphere but increases the total FACs in the winter hemisphere and their effect in the winter polar cap. *Laundal and Østgaard* [2009] reported about significant asymmetry of the auroral intensities between the northern and southern hemispheres, in particular in dusk and dawn sectors. This asymmetry was interpreted in terms of interhemispheric FACs related to seasons.

We can suggest that in our case, the observed asymmetry in plasma density fluctuations over polar regions has a seasonal aspect, i.e., local winter-local summer conditions, and subsequent difference in the particle precipitation intensity and formation of the strong FACs patterns at the edges of precipitation regions. *Fillingim et al*. [2005] reported that large-scale morphological asymmetry of the aurora can be explained by the solar wind-magnetosphere interaction when the IMF B_y component is significant. The IMF modifies the ionospheric convection pattern and lead to a hemispheric asymmetry in the Region 1 FACs. When B_Y is positive, as it was observed in our case (Figure 1), there should be a stronger upward FACs on the duskside of the southern hemisphere, as well as aurora should be brighter and more structured at the southern hemisphere. At that, *Laundal and Østgaard* [2009] suggested that differences in interhemispheric FACs can be caused by the more efficient solar wind dynamo that drives stronger high-latitude (Region 1) currents in the southern hemisphere for large positive IMF B_X. For the storm day of 30 August 2004, both IMF B_X and B_Y were largely positive (Figure 1), which could have possibly resulted in the occurrence of much stronger FACs at the high-latitude region of the southern hemisphere and subsequently increased intensity of the ionospheric plasma density irregularities.

6.2. Ionospheric Irregularities at Low Latitudes

One of the distinguished peculiarities of the geomagnetic storm of 30 August 2004 was in long-lasting main phase, from 00 UT to 22 UT on 30 August 2004 (Figure 1). The IMF B_Z component was negative from 09 to 23 UT on 30 August, and minimal values of the IMF B_Z were observed during the period of 19–23 UT. *Huang et al*. [2005] showed that in cases when the IMF B_Z remains southward for several hours and the magnetic activity continues to intensify, the penetration of the electric field into the low-latitude ionosphere may persist for many hours without attenuation. It is assumed that storm time penetration electric fields associated with the southward IMF during the main phase of magnetic storms are eastward on the dayside and drives the equatorial F region to move upward, reinforcing, together with neutral winds, the equatorial fountain effect [e.g., *Tsurutani et al*., 2004; *Mannucci et al*., 2005, 2014; *Astafyeva*, 2009a, 2009b; *Balan et al*., 2009, 2010]; consequently, this effect produces favorable conditions for the excitation of the R-T instability [e.g., *Kelley*, 1985; *Fejer et al*., 1999; *Huang et al*., 2001; *Basu et al*., 2007; *Huang*, 2011]. When the lifted F region reaches the height where the ion-neutral collision frequency is small enough, the R-T instability will rapidly grow, resulting in the generation of equatorial spread F events [e.g., *Farley et al*., 1970; *Jayachandran et al*., 1993]. *Huang et al*. [2001] reported that topside plasma of the Atlantic sector is more R-T unstable than that in the Pacific and more bubbles can be generated after sunset in the weak magnetic field of the Atlantic sector. We suggest that during the prolonged main geomagnetic storm, the enhanced eastward electric field caused the uplift of the F layer at postsunset local time in the Atlantic sector; this uplift was recognized in the form of the EIA reintensification at the dusk, large enhancements of the topside electron density at the crests of the EIA [*Astafyeva et al*., 2015], and formation of significant plasma depletions and irregularities over rather large longitudinal range.

We found rather large and broad plasma density depletions in the meridional direction by CHAMP Ne observations that were accompanied by the simultaneous increase of CHAMP ROTI values. These broad depletions can be explained by the field-aligned extent of the equatorial plasma bubbles, as plasma bubbles can ascend to thousands of kilometers at their apex, and the depleted density regions can extend even into the middle latitudes along the geomagnetic field lines [e.g., *Dyson and Benson*, 1978; *Burke et al*., 1979; *Kelley et al*., 2011].

Rather interesting moment is the detection of the equatorial ionospheric irregularities in the form of plasma density depletions in the morning sector on 31 August 2004. Generally, equatorial plasma irregularities have

been regarded as postsunset phenomena, whereas reported postsunrise equatorial irregularities are rather scarce [e.g., *Burke et al.*, 1979; *Gentile et al.*, 2011]. New results on the detection of plasma density depletions with embedded irregularities at dawn sector were found with the recent C/NOFS mission; these deep presunrise depletions are observed under quiet time close to *E* region terminator and are associated with upward plasma drifts [*de La Beaujardiere et al.*, 2009]. *Huang et al.* [2013] reported about C/NOFS observation of the equatorial plasma bubbles that persisted from 02 LT to 14–15 LT during moderate geomagnetic storm; generation of the bubbles were related to storm time disturbance dynamo process and overshielding electric fields. *Hysell and Burcham* [2002] also observed strong equatorial irregularities between 04 and 06 LT for the day with high *Kp* values (geomagnetic storm). *Fejer et al.* [1999] studied the late night spread *F*, occurred most often between 04 and 06 LT, and noted that spread *F* can occasionally last into the daylight hours under the conditions of the geomagnetic storm. *Li et al.* [2012] reported about the detection of the postsunrise intense ionospheric irregularities at low to middle latitudes at the recovery phase of the magnetic storm. These irregularities were detected in GPS TEC measurements from Japan GPS network (GPS Earth Observation Network System) from ~05 LT to ~11 LT. It was suggested that the long-time existence of the irregularities after sunrise can be related to the daytime intense negative ionospheric storm on 21 March 2001. Our results demonstrate the occurrence of the morning-time plasma density irregularities at the recovery phase of a moderate storm. These irregularities were detected at ~08–09 LT simultaneously in both CHAMP ROTI and CHAMP Ne observations. This local time is far from the sunrise terminator and occurrence of the strong equatorial spread *F* can be related primarily with storm time disturbance dynamo [*Fejer et al.*, 1999]. The patterns of the ionospheric irregularity occurrence in CHAMP ROTI observations are rather similar to those of the CHAMP Ne; however, the irregularities were detected at different altitudes: orbit plane versus topside ionosphere above the orbit. We can also emphasize the advantage of the use of the satellite measurements for irregularities detection; as in the given case, they were found over the Pacific ocean where the presence of ground-based instruments is not possible.

6.3. Comparison of CHAMP ROTI With the In Situ Ne Measurements (RODI)

We found that CHAMP ROTI technique can be successfully used as additional data source to study the ionospheric irregularities together with standard ionospheric probe observations. Although these two measurements are quite different and detect irregularities at the different spatial and altitudinal scales, in the case when the present or forthcoming LEO mission's payload does not have the in situ plasma probe, the data of a spaceborne GPS receiver can be expected to be used solo for this task.

In order to demonstrate the general similarities and differences of CHAMP ROTI with the in situ measurements, we process the CHAMP in situ data and obtain in the similar way values of CHAMP ROD (rate of density) in units of 10^5 el/(cm^3/min) and CHAMP RODI (ROD index), based on the standard deviation of the ROD and calculated over 1 min period with running window. Figure 9a shows the comparison of global maps with CHAMP ROTI and CHAMP RODI observations along the satellite passes for the evening sector on 30 August 2004. The measurements units are different, but color scale for the ROTI/RODI intensity is the same. Similarities in geographical location of the ionospheric irregularities, detected by independent ROTI and RODI techniques along the CHAMP passes, are clearly visible. The same high- and low-latitude regions are affected by the occurrence of the intense ionospheric irregularities; however, further comparison shows that the RODI has relatively larger values with respect to the ROTI map for several parts of passes over the equatorial regions, whereas, on the contrary, the ROTI map shows relatively larger values at high-latitude region.

To further study the relationship between the ROTI and RODI values, we analyze CHAMP data for 7 quiet days before the storm and for the disturbed day of 30 August 2004. We process data for the evening and morning sectors together and bin results into two specific regions of high latitudes (MLAT > 55°) and low latitudes ($-25 <$ MLAT < 25). Figure 9b presents a comparison of the ROTI versus RODI distribution for the high- and low-latitude regions and quiet and disturbed conditions. As one can see, these two independent measurements are highly correlated. For high latitudes, we observe smaller values during quiet conditions and significant increase of both ROTI and RODI values during the geomagnetic storm that can be explained by the occurrence of structures with much stronger electron density gradients in the high-latitude ionosphere during storm. For low latitudes, high values of ROTI and RODI are observed at quiet and disturbed times, which can be attributed to the regular postsunset equatorial irregularities. For the day of the storm, the correlation coefficient reached 0.80 for high latitudes and 0.85 for low latitudes. It is interesting to note the difference between the two selected
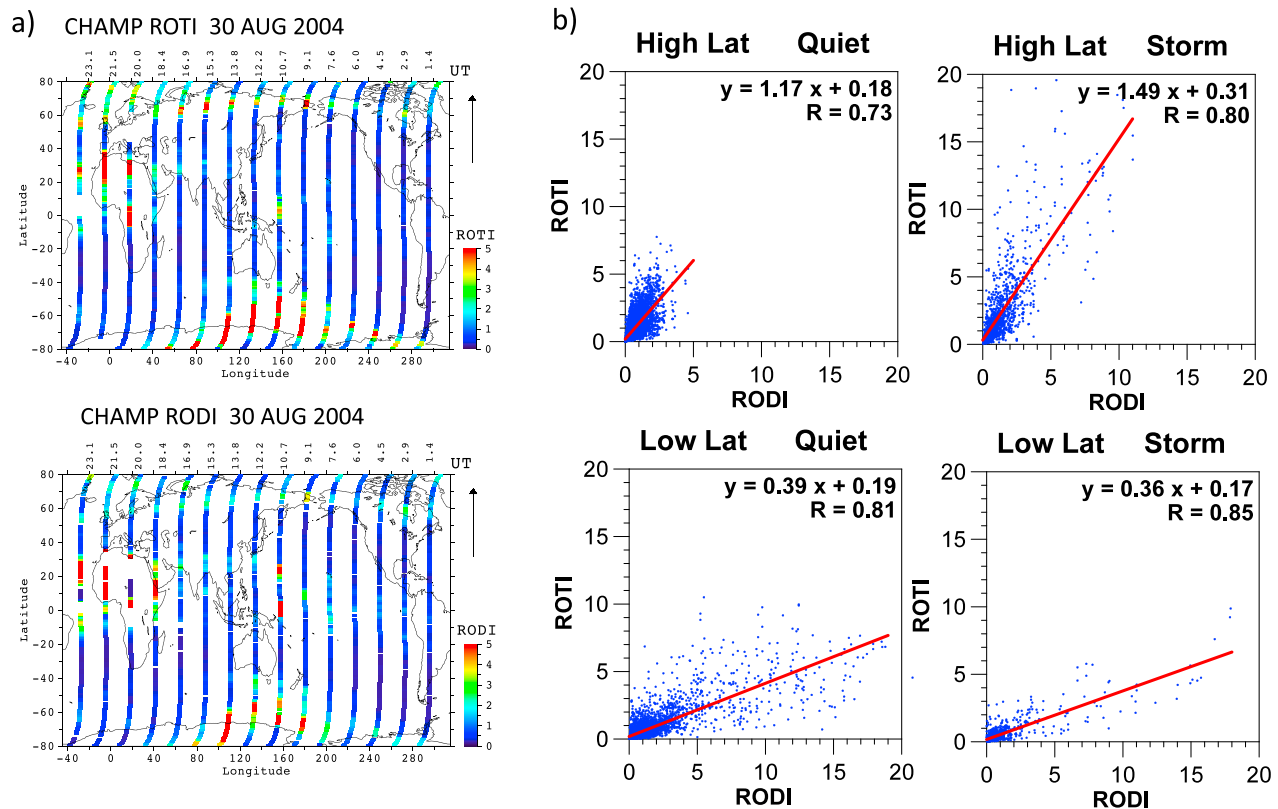
Figure 9. Comparison of CHAMP ROTI and CHAMP RODI observations: (a) global maps of the ROTI and RODI variability along CHAMP passes on 30 August 2004 for evening sector and (b) scatterplots of ROTI versus RODI distributions for quiet conditions and disturbed day of 30 August 2004. The red line corresponds to the best fit line. CHAMP ROTI values are in units of TECU/min, that is equal to 10^{12} el/(cm^2/min), CHAMP RODI in 10^5 el/(cm^3/min).

regions—for high latitudes, CHAMP ROTI had the tendency to be higher than CHAMP RODI values (slopes of 1.17 and 1.49), whereas at low latitudes, the opposite situation is observed (slopes of 0.39 and 0.36), where RODI values had higher values in ROTI-RODI pairs.

The obtained results confirm relatively high correlation between the CHAMP ROTI and CHAMP in situ data (RODI), which can be explained by the occurrence of the most intense ionospheric irregularities near the altitude of the CHAMP satellite. However, we should note the principal difference between the GPS and in situ techniques. In fact, the in situ measurements is a kind of 1-D punctual measurements along the CHAMP pass, as it is a specific single Ne value per moment of time at the fixed and known altitude. At the same time, CHAMP GPS TEC technique relates to the kind of 2-D measurements as GPS rays intersect the space between LEO altitude and GPS orbits at 20,200 km, and due to ability of simultaneous tracking of several GPS satellites, it can scan relatively large area of the topside ionosphere, but it provides only 1 integral TEC value along one ray, and we do not able to determine the precise altitude of the detected irregularities; it can be any altitude higher than LEO orbit. However, as ROTI values can be averaged for different visible GPS rays, this value can represent the irregularities occurrence over much larger spatial area than punctual measurements.

The eventual resemblance or difference between these two techniques would depend essentially on the altitudinal extent of plasma irregularities as well as the altitudinal distribution of the background ionospheric plasma density at different latitudinal regions. Thus, *Hysell and Burcham* [1998, 2002] separated four main categories of equatorial irregularities: bottom-type layers, bottomside layers, topside layers (radar plumes), and postmidnight irregularities. The latter two categories represent large-scale, deep plasma depletions that break through to the topside and rapidly ascend to high altitudes. In connection with classification, we can consider several cases of the simultaneous detection of ionospheric irregularities by using both ROTI and RODI techniques: (1) Bottomside irregularities are observed by the in situ measurements but cannot be de detected by the upward looking GPS antenna. (2) Topside irregularities cannot be detected by the in situ

measurements while they are clearly visible in the POD TEC. (3) Largely extended irregularities can be detected by both techniques, but the intensity may differ with the altitudinal distribution/position of irregularities as compared to the orbital height of the satellite. Therefore, we can conclude that, in general, the interchangeability of these techniques cannot be extended to all cases. Besides, so far, there is no available technique to resolve temporal and spatial variability of the *F* region and topside plasma irregularities on a global scale, and only a combination of several data sources is the mostly accepted way to study the ionospheric irregularities, and LEO ROTI technique could add valuable information to this research.

7. Conclusions

We used CHAMP, DMSP, and ground-based GPS observations to examine the occurrence of the topside ionospheric irregularities during the main phase of the geomagnetic storm of 29–31 August 2004. Although far from the most intense storms of the year 2004, this storm was particular because of unusually long-time substorm activity and prolonged particle precipitation that led to the development of the intense ionospheric irregularities. One of the highlights of the present study is the use of multisatellite observations to investigate the structure of the ionospheric irregularities on the global scale. For the first time, we show that a global distribution of ionospheric irregularities caused the phase fluctuations in GPS measurements from LEO CHAMP satellite. Application of ROTI technique to LEO GPS data shows its sensibility even to a rather moderate geomagnetic storm. We show that the LEO ROTI technique allows to successfully detect the electron density irregularities at the topside ionosphere above the CHAMP orbit from GPS signal measurements under geomagnetically quiet and disturbed conditions. Our comparison of the LEO ROTI technique with independent in situ measurements confirmed the reliability of this approach but also showed that despite major similarities, there can be significant discrepancies between these two techniques. Due to the availability of GPS POD data derived from multisatellite missions like FORMOSAT-3/COSMIC and Swarm, ROTI technique based on topside LEO GPS measurements could essentially contribute to a global space weather monitoring system and provide a valuable database to study the ionospheric irregularities occurrence.

References

Aarons, J., and B. Lin (1999), Development of high latitude phase fluctuations during the January 10, April 10–11, and May 15, 1997 magnetic storms, *J. Atmos. Sol. Terr. Phys.*, *61*(3–4), 309–327.

Akasofu, S.-I. (1968), *Polar and Magnetospheric Substorms*, p. 280, D. Reidel, Dordrecht, Netherlands.

Astafyeva, E. (2009a), Effects of strong IMF B_z southward events on the equatorial and mid-latitude ionosphere, *Ann. Geophys.*, *27*, 1175–1187, doi:10.5194/angeo-27-1175-200.

Astafyeva, E. (2009b), Dayside ionospheric uplift during strong geomagnetic storms as detected by the CHAMP, SAC-C, TOPEX, and Jason-1 satellites, *Adv. Space Res.*, *43*, 1749–1756, doi:10.1016/j.asr.2008.09.036.

Astafyeva, E., Y. Yasyukevich, A. Maksikov, and I. Zhivetiev (2014), Geomagnetic storms, super-storms, and their impacts on GPS-based navigation systems, *Space Weather*, *12*, 508–525, doi:10.1002/2014SW001072.

Astafyeva, E., I. Zakharenkova, and E. Doornbos (2015), Opposite hemispheric asymmetries during the ionospheric storm of 29–31 August 2004, *J. Geophys. Res. Space Physics*, *120*, doi:10.1002/2014JA020710, in press.

Balan, N., H. Alleyne, Y. Otsuka, D. Vijaya Lekshmi, B. G. Fejer, and I. McCrea (2009), Relative effects of electric field and neutral wind on positive ionospheric storms, *Earth Planets Space*, *61*, 439–445.

Balan, N., K. Shiokawa, Y. Otsuka, T. Kikuchi, D. Vijaya Lekshmi, S. Kawamura, M. Yamamoto, and G. J. Bailey (2010), A physical mechanism of positive ionospheric storms at low latitudes and midlatitudes, *J. Geophys. Res.*, *115*, A02304, doi:10.1029/2009JA014515.

Basu, S., S. Basu, F. J. Rich, K. M. Groves, E. MacKenzie, C. Coker, Y. Sahai, P. R. Fagundes, and F. Becker-Guedes (2007), Response of the equatorial ionosphere at dusk to penetration electric fields during intense magnetic storms, *J. Geophys. Res.*, *112*, A08308, doi:10.1029/2006JA012192.

Blewitt, G. (1990), An automatic editing algorithm for GPS data, *Geophys. Res. Lett.*, *17*, 199–202, doi:10.1029/GL017i003p00199.

Burke, W. J., R. C. Sagalyn, R. G. Rastogi, M. Ahmed, F. J. Rich, D. E. Donatelli, and P. J. L. Wildman (1979), Postsunrise refilling of the low-latitude topside ionosphere, *J. Geophys. Res.*, *84*, 4201–4206, doi:10.1029/JA084iA08p04201.

Cherniak, I., A. Krankowski, and I. Zakharenkova (2014), Observation of the ionospheric irregularities over the northern hemisphere: Methodology and Service, *Radio Sci.*, *49*, 653–662, doi:10.1002/2014RS005433.

de La Beaujardiere, O., J. M. Retterer, R. F. Pfaff, P. A. Roddy, C. Roth, W. J. Burke, and D. L. Cooke (2009), C/NOFS observations of deep plasma depletions at dawn, *Geophys. Res. Lett.*, *36*, L00C06, doi:10.1029/2009GL038884.

Dyson, P. L., and R. F. Benson (1978), Topside sounder observations of equatorial bubbles, *Geophys. Res. Lett.*, *5*(9), 795–798, doi:10.1029/GL005i009p00795.

Echer, E., W. D. Gonzalez, B. T. Tsurutani, and A. L. C. Gonzalez (2008), Interplanetary conditions causing intense geomagnetic storms ($Dst \leq -100$ nT) during solar cycle 23 (1996–2006), *J. Geophys. Res.*, *113*, A05221, doi:10.1029/2007JA012744.

Farley, D. T., B. B. Balsley, R. F. Woodman, and J. P. Mc-Clure (1970), Equatorial spread *F*: Implications of VHF radar observations, *J. Geophys. Res.*, *75*, 7199–7216, doi:10.1029/JA075i034p07199.

Fejer, B. G., and M. C. Kelley (1980), Ionospheric irregularities, *Rev. Geophys. Space Phys.*, *18*(2), 401–454.

Fejer, B. G., L. Scherliess, and E. R. de Paula (1999), Effects of the vertical plasma drift velocity on the generation and evolution of equatorial spread *F*, *J. Geophys. Res.*, *104*(A9), 19,859–19,869, doi:10.1029/1999JA900271.

Fillingim, M. O., G. K. Parks, H. U. Frey, T. J. Immel, and S. B. Mende (2005), Hemispheric asymmetry of the afternoon electron aurora, *Geophys. Res. Lett.*, *32*, L03113, doi:10.1029/2004GL021635.

Gentile, L. C., W. J. Burke, P. A. Roddy, J. M. Retterer, and R. T. Tsunoda (2011), Climatology of plasma density depletions observed by DMSP in the dawn sector, *J. Geophys. Res.*, *116*, A03321, doi:10.1029/2010JA016176.

Gonzalez, W. D., J. A. Joselyn, Y. Kamide, H. W. Kroehl, G. Rostoker, B. T. Tsurutani, and V. M. Vasyliunas (1994), What is a geomagnetic storm?, *J. Geophys. Res.*, *99*(A4), 5771–5792, doi:10.1029/93JA02867.

Heise, S., N. Jakowski, A. Wehrenpfennig, C. Reigber, and H. Lu (2002), Sounding of the topside ionosphere/plasmasphere based on GPS measurements from CHAMP: Initial results, *Geophys. Res. Lett.*, *29*(14), 1699, doi:10.1029/2002GL014738.

Hofmann-Wellenhof, B. (2001), *Global Positioning System: Theory and Practice*, Springer, New York.

Huang, C.-S. (2011), Occurrence of equatorial plasma bubbles during intense magnetic storms, *Int. J. Geophys.*, doi:10.1155/2011/401858.

Huang, C.-S., J. C. Foster, L. P. Goncharenko, P. J. Erickson, W. Rideout, and A. J. Coster (2005), A strong positive phase of ionospheric storms observed by the Millstone Hill incoherent scatter radar and global GPS network, *J. Geophys. Res.*, *110*, A06303, doi:10.1029/2004JA010865.

Huang, C.-S., O. de La Beaujardiere, P. A. Roddy, D. E. Hunton, J. O. Ballenthin, and M. R. Hairston (2013), Long-lasting daytime equatorial plasma bubbles observed by the C/NOFS satellite, *J. Geophys. Res. Space Physics*, *118*, 2398–2408, doi:10.1002/jgra.50252.

Huang, C. Y., W. J. Burke, J. S. Machuzak, L. C. Gentile, and P. J. Sultan (2001), DMSP observations of equatorial plasma bubbles in the topside ionosphere near solar maximum, *J. Geophys. Res.*, *106*(A5), 8131–8142, doi:10.1029/2000JA000319.

Hysell, D. L., and J. D. Burcham (1998), JULIA radar studies of equatorial spread *F*, *J. Geophys. Res.*, *103*(A12), 29,155–29,167, doi:10.1029/98JA02655.

Hysell, D. L., and J. D. Burcham (2002), Long term studies of equatorial spread *F* using the JULIA radar at Jicamarca, *J. Atmos. Sol. Terr. Phys.*, *64*(12–14), 1531–1543, doi:10.1016/S1364-6826(02)00091-3.

Hysell, D. L., H. C. Aveiro, and J. L. Chau (2013), Ionospheric irregularities: Frontiers, *Geophys. Monogr. Ser.*, *201*, 217–240.

Jakowski, N., Y. Beniguel, G. De Franceschi, M. H. Pajares, K. S. Jacobsen, I. Stanislawska, L. Tomasik, R. Warnant, and G. Wautelet (2012), Monitoring, tracking, and forecasting ionospheric perturbations using GNSS techniques, *J. Space Weather Space Clim.*, *2*, A22, doi:10.1051/swsc/2012022.

Jayachandran, B., N. Balan, P. B. Rao, J. H. Sastri, and G. J. Bailey (1993), HF Doppler and ionosonde observations on the onset conditions of equatorial spread *F*, *J. Geophys. Res.*, *98*(8), 13,741–13,750, doi:10.1029/93JA00302.

Kelley, M. C. (1985), Equatorial spread *F*: Recent results and outstanding problems, *J. Atmos. Sol. Terr. Phys.*, *47*, 745–752.

Kelley, M. C., J. J. Makela, O. Beaujardiere, and J. Retterer (2011), Convective ionospheric storms: A review, *Rev. Geophys.*, *49*, RG2003, doi:10.1029/2010RG000340.

Kersley, L., C. D. Russel, and D. L. Rice (1995), Phase scintillations and irregularities in the northern polar ionosphere, *Radio Sci.*, *30*, 619–629, doi:10.1029/94RS03175.

Keskinen, M. J., and S. L. Ossakow (1983), Theories of high-latitude ionospheric irregularities: A review, *Radio Sci.*, *18*(6), 1077–1091, doi:10.1029/RS018i006p01077.

Keskinen, M., S. Ossakow, and P. Chaturvedi (1980), Preliminary report of numerical simulations of intermediate wavelength collisional Rayleigh-Taylor instability in equatorial spread *F*, *J. Geophys. Res.*, *85*(A4), 1775–1778, doi:10.1029/JA085iA04p01775.

Kuo, F. S., S. Y. Chou, and S. J. Shan (1998), Comparison of topside and bottomside irregularities in equatorial *F* region ionosphere, *J. Geophys. Res.*, *103*, 2193–2199, doi:10.1029/97JA02586.

Laundal, K. M., and N. Østgaard (2009), Asymmetric auroral intensities in the Earth's Northern and Southern Hemispheres, *Nature*, *460*, 491–493, doi:10.1038/nature08154.

Lazutin, L. L., M. I. Panasyuk, and N. Hasebe (2011), Acceleration and losses of energetic protons and electrons during magnetic storm on August 30–31, 2004, *Cosmic Res.*, *49*(1), 35–41.

Li, J., G. Ma, T. Maruyama, and Z. Liu (2012), Mid-latitude ionospheric irregularities persisting into late morning during the magnetic storm on 19 March 2001, *J. Geophys. Res.*, *117*, A08304, doi:10.1029/2012JA017626.

Liou, K., P. T. Newell, and C.-I. Meng (2001), Seasonal effects on auroral particle acceleration and precipitation, *J. Geophys. Res.*, *106*, 5531–5542, doi:10.1029/1999JA000391.

Lyatskaya, S., W. Lyatsky, and G. V. Khazanov (2008), Relationship between substorm activity and magnetic disturbances in the two polar caps, *Geophys. Res. Lett.*, *35*, L20104, doi:10.1029/2008GL035187.

Ma, G., and T. Maruyama (2003), Derivation of TEC and estimation of instrumental biases from GEONET in Japan, *Ann. Geophys.*, *21*(10), 2083–2093.

Mannucci, A. J., B. T. Tsurutani, B. A. Iijima, A. Komjathy, A. Saito, W. D. Gonzalez, F. L. Guarnieri, J. U. Kozyra, and R. Skoug (2005), Dayside global ionospheric response to the major interplanetary events of October 29–30, 2003 "Halloween Storms", *Geophys. Res. Lett.*, *32*, L12S02, doi:10.1029/2004GL021467.

Mannucci, A. J., G. Crowley, B. T. Tsurutani, O. P. Verkhoglyadova, A. Komjathy, and P. Stephens (2014), Interplanetary magnetic field B_Y control of prompt total electron content increases during superstorms, *J. Atmos. Sol. Terr. Phys.*, *115–116*, 7–16, doi:10.1016/j.jastp.2014.01.001.

Maruyama, T., G. Ma, and T. Tsugawa (2013), Storm-induced plasma stream in the low-latitude to mid-latitude ionosphere, *J. Geophys. Res. Space Physics*, *118*, 5931–5941, doi:10.1002/jgra.50541.

Newell, P. T., V. A. Sergeev, G. R. Bikkuzina, and S. Wing (1998), Characterizing the state of the magnetosphere: Testing the ion precipitation maxima latitude (b2i) and the ion isotropy boundary, *J. Geophys. Res.*, *103*, 4739–4746, doi:10.1029/97JA03622.

Nishioka, M., A. Saito, and T. Tsugawa (2008), Occurrence characteristics of plasma bubble derived from global ground-based GPS receiver networks, *J. Geophys. Res.*, *113*, A05301, doi:10.1029/2007JA012605.

Ossakow, S. L. (1981), Spread *F* theories: A review, *J. Atmos. Sol. Terr. Phys.*, *43*, 437–452.

Phelps, A. D. R., and R. C. Sagalyn (1976), Plasma density irregularities in the high-latitude top side ionosphere, *J. Geophys. Res.*, *81*(4), 515–523, doi:10.1029/JA081i004p00515.

Pi, X., A. J. Mannucci, U. J. Lindqwister, and C. M. Ho (1997), Monitoring of global ionospheric irregularities using the worldwide GPS network, *Geophys. Res. Lett.*, *24*, 2283–2286, doi:10.1029/97GL02273.

Reigber, C., H. Lühr, and P. Schwintzer (2002), CHAMP mission status, *Adv. Space Res.*, *30*(2), 129–134.

Rodger, A., and M. Jarvis (2000), Ionospheric research 50 years ago, today, and tomorrow, *J. Atmos. Sol. Terr. Phys.*, *62*(17–18), 1629–1645, doi:10.1016/S1364-6826(00)00116-4.

Rodger, A. S., R. J. Moffett, and S. Quegan (1992), The role of ion drift in the formation of ionisation troughs in the mid- and high-latitude ionosphere: A review, *J. Atmos. Sol. Terr. Phys.*, *54*(1), 1–30.

Su, S.-Y., C. H. Liu, H. H. Ho, and C. K. Chao (2006), Distribution characteristics of topside ionospheric density irregularities: Equatorial versus midlatitude regions, *J. Geophys. Res.*, *111*, A06305, doi:10.1029/2005JA011330.

Tsurutani, B., et al. (2004), Global dayside ionospheric uplift and enhancement associated with interplanetary electric fields, *J. Geophys. Res.*, *109*, A08302, doi:10.1029/2003JA010342.

Woodman, R. F. (1993), Equatorial ionospheric irregularities as observed by Jicamarca radar, in *Low-Latitude Ionospheric Physics*, *COSPAR Colloq. Ser.*, vol. 7, pp. 83–95, Elsevier, Oxford, U. K.

Yagodkina, O. I., I. V. Despirak, and V. G. Vorobjev (2012), Spatial distribution of auroral precipitation during storms caused by magnetic clouds, *J. Atmos. Sol. Terr. Phys.*, *77*, 1–18, doi:10.1016/j.jastp.2011.06.009.

Yizengaw, E., M. B. Moldwin, A. Komjathy, and A. J. Mannucci (2006), Unusual topside ionospheric density response to the November 2003 superstorm, *J. Geophys. Res.*, *111*, A02308, doi:10.1029/2005JA011433.

Yue, X., W. S. Schreiner, D. C. Hunt, C. Rocken, and Y.-H. Kuo (2011), Quantitative evaluation of the low Earth orbit satellite based slant total electron content determination, *Space Weather*, *9*, S09001, doi:10.1029/2011SW000687.